Perlinhibin, a Cysteine-, Histidine-, and Arginine-Rich Miniprotein from Abalone (*Haliotis laevigata*) Nacre, Inhibits In Vitro Calcium Carbonate Crystallization

Karlheinz Mann,* Frank Siedler,* Laura Treccani,† Fabian Heinemann,† and Monika Fritz†
*Max-Planck-Institut für Biochemie, Martinsried, Germany; and †Institut für Biophysik der Universität Bremen, Bremen, Germany

ABSTRACT We have isolated a 4.785 Da protein from the nacreous layer of the sea snail *Haliotis laevigata* (greenlip abalone) shell after demineralization with acetic acid. The sequence of 41 amino acids was determined by Edman degradation supported by mass spectrometry. The most abundant amino acids were cysteine (19.5%), histidine (17%), and arginine (14.6%). The positively charged amino acids were almost counterbalanced by negatively charged ones resulting in a calculated isoelectric point of 7.86. Atomic-force microscopy studies of the interaction of the protein with calcite surfaces in supersaturated calcium carbonate solution or calcium chloride solution showed that the protein bound specifically to calcite steps, inhibiting further crystal growth at these sites in carbonate solution and preventing crystal dissolution when carbonate was substituted with chloride. Therefore this protein was named perlinhibin. X-ray diffraction investigation of the crystal after atomic-force microscopy growth experiments showed that the formation of aragonite was induced on the calcite substrate around holes caused by perlinhibin crystal-growth inhibition. The strong interaction of the protein with calcium carbonate was also shown by vapor diffusion crystallization. In the presence of the protein, the crystal surfaces were covered with holes due to protein binding and local inhibition of crystal growth. In addition to perlinhibin, we isolated and sequenced a perlinhibin-related protein, indicating that perlinhibin may be a member of a family of closely related proteins.

INTRODUCTION

The various biominerals deposited by invertebrates invariably contain small amounts of an organic matrix consisting of proteins, glycoproteins, and polysaccharides (1,2). The organic matrix is believed to control crystal nucleation, orientation, size, and phase. The soluble matrix of mollusk shells is known to contain components that inhibit crystal growth, probably by binding to steps and kinks of crystal surfaces that are the preferred sites of crystal growth (3,4). However, only very few components of the matrix were characterized at the molecular level and molecular mechanisms are largely unknown.

The shell of the abalone consists of >95% of calcium carbonate, which is deposited as calcite in the outer (prismatic) layer of the shell and as aragonite in the inner (nacreous) layer (5,6). The organic matrix of the two layers contains different sets of proteins, which, in vitro, induce the crystallization of the same calcium carbonate polymorph with which they were originally associated and modify the growth of crystals (7,8). Some abalone nacre proteins were purified and characterized. These are comprised of the multidomain protein lustrin A (9), thought to be a component of the adhesive between nacre mineral tablets (10); C-type lectin perlucin, which promotes $CaCO_3$ crystal nucleation in vitro (11); perlustrin, a small growth factor-binding protein (12); and perlwapin, a protein containing three whey-acidic protein domains and which binds to calcite steps in vitro, inhibiting crystal growth (13). Furthermore, the acidic nacre proteins AP7, AP8α/β and AP24 have been isolated and were shown to interact with specific calcite surface structures (14,15).

Here we report the isolation and sequence analysis of perlinhibin, a new protein from abalone (*Haliotis laevigata*) nacre, and perlinhibin-related protein that showed a sequence identity to perlinhibin of 67.5%. Furthermore, the influence of perlinhibin on calcium carbonate crystallization was investigated using the atomic force microscope (AFM) to study the binding of perlinhibin to calcite surfaces in aqueous solution and by the ammonium carbonate vapor diffusion technique.

MATERIALS AND METHODS

Protein purification and sequence analysis

The aragonitic layer of *H. laevigata* shells was decalcified with acetic acid and the soluble proteins were separated by ion exchange chromatography (16). This yielded a mixture of small proteins which was further separated by reversed phase HPLC using a short C4 column (214TP5405, 4.6 × 50 mm; Vydac, Columbia, MD) with a gradient of 10–80% solvent B (70% acetonitrile in 0.1% trifluoroacetic acid) in 60 min at a flow rate of 0.5 ml/min. The resulting peaks were searched for new proteins by N-terminal sequence analysis. Before determination of complete sequences, the purified proteins were dissolved (1 mg/ml) in 0.1 M Tris, pH 8.5, 6 M guanidinium hydrochloride and reduced with 10 μl mercaptoethanol for 6 h at 50°C. After cooling to room temperature 20 μl vinylpyridine was added and the mixture was kept at room temperature in the dark overnight. Reagents and buffer were removed by reversed phase HPLC as above. Perlinhibin was cleaved with cyanogen bromide in 70% formic acid by addition of a small crystal of CNBr and incubation at room temperature overnight in the dark. The fragments were separated using a Superdex Peptide column (HR10/30; Pharmacia

Submitted November 8, 2006, and accepted for publication April 12, 2007.

Address reprint requests to M. Fritz, Tel.: 04-21-218-3458; E-mail: mf@biophysik.uni-bremen.de.

Editor: Marcia Newcomer.

0006-3495/07/08/1246/09 $2.00

doi: 10.1529/biophysj.106.100636

Biotech, Uppsala, Sweden) in 0.1% trifluoroacetic acid, 25% acetonitrile, at a flow rate of 0.3 ml/min. The perlinhibin-related protein was cleaved with endoproteinase Arg-C (sequencing grade; Roche Molecular Biochemicals, Indianapolis, IN) in 0.1 M ammonium hydrogen carbonate, 4 M urea, 5 mM dithiothreitol, 0.5 mM EDTA, at an enzyme to substrate ratio of 1:100 for 6 h at 23°C. The resulting fragments were separated by reversed phase HPLC using a C18 column (238TP53, 3.2 × 250 mm; Vydac) with a linear gradient of 5–60% solvent B in 160 min at a flow rate of 0.25 ml/min. Proteins and fragments were sequenced using sequencers 473 A and 492 Z (Applied Biosystems, Foster City, CA). Electrospray ionization mass spectrometry was done with an API 365 (PE Sciex, Foster City, CA).

Preparation of saturated calcium carbonate

Saturated $CaCO_3$ solution was prepared according to Hillner et al. (17). Thirty to fifty milliliters of 100 mM $NaHCO_3$ was added slowly to 120 ml of 40 mM $CaCl_2$ with continuous stirring until the solution started to become turbid. The final pH was adjusted to 8.2 with 1 M NaOH. The solution was filtered sterile through a filter with pores of 0.22 μm (Durapore 0.22 μm membrane filter; Millipore, Billerica, MA) and 0.02% NaN_3 was added to prevent microbial growth.

Perlinhibin in saturated calcium carbonate and sodium chloride solution

Eight milliliters of perlinhibin solution, stored in 20 mM citrate buffer (pH 4.8), was concentrated in a speed vac concentrator (Savant Speed Vac; Schütt Labortechnik, Göttingen, Germany) to a final volume of ~2 ml and dialyzed three times against 100 ml of saturated $CaCO_3$ solution at 4°C. The dialysis tubing (Spectra/Por Membrane MWCO: 6–8.000; Spectrum Medical Industries, Houston, TX) was boiled in 7 mM EDTA (Karl Roth, Karlsruhe, Germany) for 5 min and then rinsed several times with deionized water before use. Protein concentration was determined with the Bradford microassay (Bio-Rad Laboratories, Hercules, CA) using IgG and BSA as standard proteins (Sigma Aldrich Chemie, Munich, Germany) and adjusted to 0.02 mg perlinhibin/ml.

For experiments under dissolution-promoting conditions, freeze-dried perlinhibin was dissolved in a sterile 7.5 mM $CaCl_2$ solution, pH 7.5, to a final concentration of 0.2 mg/ml and stored at 4°C.

AFM imaging

AFM imaging was performed in contact-mode with a commercial system (Nanoscope IIIa Multimode; Digital Instruments, Santa Barbara, CA) equipped with a piezoelectric scanner. Silicon nitride (Si_3N_4) cantilevers (Microlevers; Park Scientific Instruments, Sunnyvale, CA) with oxide-sharpened tips were used after treatment with UV light for 10 min to destroy organic contaminants on the tip. Cantilevers with a nominal force constant of 0.01 N/m were chosen for imaging. The glass fluid cell and the silicon O-ring were cleaned with a specific detergent (Ultra Joy; Procter & Gamble, Cincinnati, OH), rinsed with deionized water and dried with compressed nitrogen before experiments.

Freshly cleaved calcite surfaces for AFM investigations [4 $\bar{4}$ $\bar{1}$ plane] were cut from a block of geological calcite of optical quality (Creel, Mexico; Kristalldruse, Munich, Germany) using a razor blade. The calcite crystals were handled with tweezers to avoid contamination of the surface and examined with an optical microscope. Fragments that presented a flat surface were glued with two-component epoxy glue (Bindulin-Werk; H.L. Schönleber, Fürth, Germany) onto clean mica plates that had been glued onto a magnetic steel disk before (12 mm diameter). The dry calcite sample was carefully rinsed with deionized water to remove calcite dust particles from the cleavage site before it was positioned at the top of the scanner. Deionized water, saturated $CaCO_3$ solution (pH 8.2), or 7.5mM $CaCl_2$ solution with and without perlinhibin, were injected directly into the fluid cell using a 1-ml, fine dosage syringe (Injekt-F 1 mL; Braun, Melsungen, Germany). All solutions were degassed and adjusted to room temperature before use to prevent the formation of air bubbles in the fluid cell during imaging. All AFM deflection images were processed with the freeware analysis software Image SXM (Ver. 1.74) for contrast adjustment and examination of height profile.

X-ray diffraction

After AFM investigation, the calcite crystal incubated with the calcium carbonate solution supplemented with perlinhibin (0.02 mg/ml) was dried at room temperature and carefully removed from the sample holder. The resulting crystal (size ~1.5 × 1.5 × 1 mm) was investigated by x-ray diffraction without any further modification, with the previously AFM-investigated surface on top, using Cu K_α radiation in Bragg-Brentano geometry.

Crystallization experiments with ammonium carbonate vapor diffusion technique

The experiments were performed following a standard procedure (4). Glass cover slides were cleaned in a solution of 70% H_2SO_4 and 30% H_2O_2 for 20 min, then rinsed several times with deionized water in an ultrasonicator, dried in an oven at 100°C and finally cooled down to room temperature before use. The cover slides were placed in a Nunc multidish (Nalge Nunc, Rochester, NY). Perlinhibin, stored in 20 mM citrate buffer (pH 4.8), was dialyzed three times (Spectra/Por Membrane MWCO: 6–8.000; Spectrum Medical Industries) at 4°C against a 7.5 mM $CaCl_2$ solution adjusted to pH 7.5 with 1 M NaOH. The final protein concentration was adjusted to 0.02 mg/ml. Wells containing the cover slides were filled with the perlinhibin solution. As a control, a well was filled with 800 μl of 7.5 mM $CaCl_2$ (pH 7.5).

The Nunc multidish was covered with a hole-dotted aluminum foil to slow down diffusion and put into an airtight desiccator (volume 25l) containing a beaker filled with ammonium carbonate. After five days of incubation at room temperature, the cover slides were gently rinsed with deionized water and dried at room temperature. The solutions were filtered sterile before use (Durapore 0.22 μm membrane filter; Millipore). Scanning electron microscope (SEM) investigation was performed using a Camscan Series 2 system (Cambridge Scientific Instruments, Ely, UK). The cover slides were glued on SEM stubs and sputter-coated with gold. Sputtering was performed with an Emitech K550 system (EM Technologies, Bonneville, FR) with a current of 10–20 mA in a 0.2 mbar argon atmosphere. SEM investigation was carried out at 20 kV in secondary or back-scattered electron imaging mode.

RESULTS

Isolation and amino-acid sequence of perlinhibin

Perlinhibin was isolated by reversed phase chromatography from the soluble matrix fraction, which also contained perlucin and perlustrin (11,16). The protein eluted as one of the first peaks and was shown by amino-acid sequence analysis to be pure. The yield was ~3 μg/shell. Mass determination of the new protein by ESI-MS yielded a major peak with a mass of 4785.2 Da and a less intense peak with a mass of 4800.8 Da (Fig. 1). The difference of 15.6 Da between these two peaks suggested the heavier species to be an oxidation product of the lighter one. These masses indicated a length of 40–45 amino acids for this novel polypeptide. This is a length that can normally be sequenced in a single Edman degradation run. However, with this peptide the repetitive yield decreased dramatically after Pro^{33} (see Fig. 3) and a significant overlap into the next cycles developed and made an unequivocal

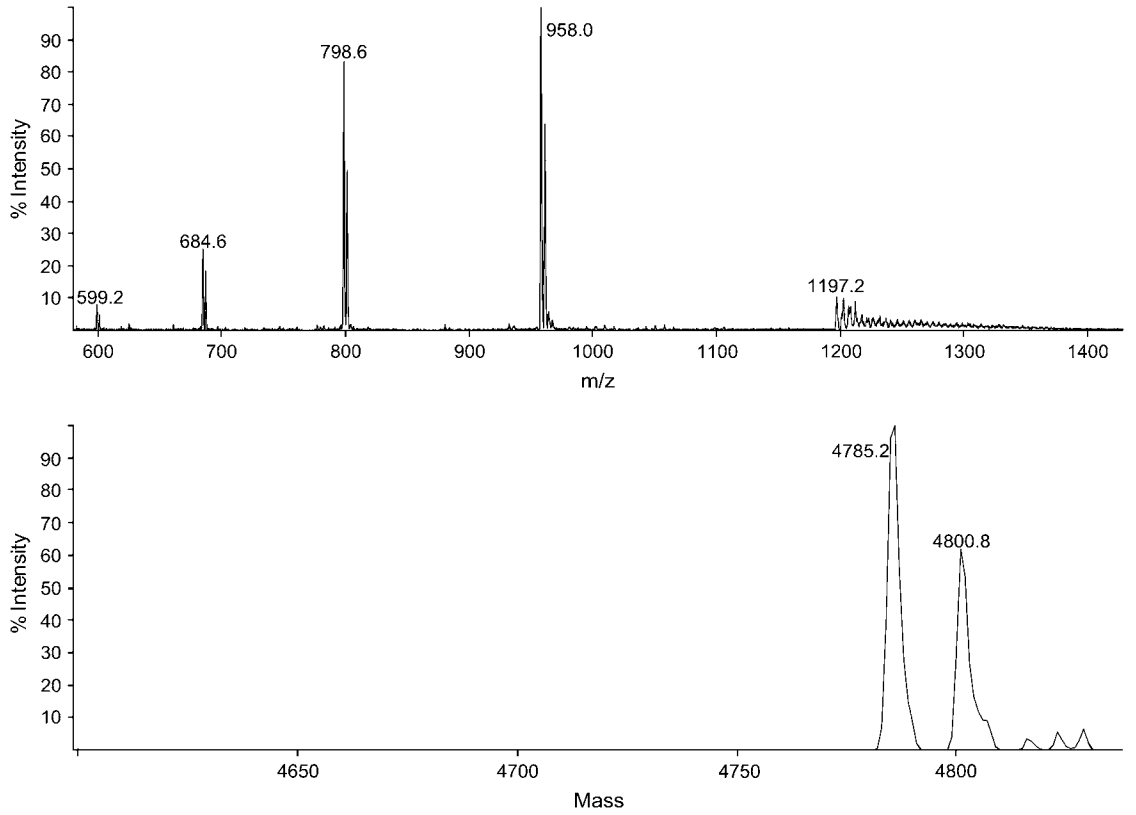

FIGURE 1 Mass determination of native perlinhibin. The upper panel shows the measured ions, the lower panel shows the deconvoluted spectrum. The peak at 4800.8 Da is an oxidation product of the 4785.2 Da species (see text).

identification of the rest of the sequence impossible. Because of these difficulties the reduced and pyridylethylated protein was cleaved with CNBr and the cleavage products were separated from each other by size exclusion chromatography using a Superdex Peptide column. The separation yielded three peaks (Fig. 2). The first peak showed a mass of 5649.8 Da, indicating that this was the uncleaved polypeptide with eight pyridylethylated cysteines and that it was derived from the oxidized native form (4800.6 Da + 8 × 105 Da = 5640.8 Da). The residual difference of 9 Da showed that the eight cysteines formed disulfide bridges in the native polypeptide (−8 Da in the native form). The most plausible explanation for the resistance of this species against CNBr cleavage was that the oxidation inferred from mass determination had taken place at Met^{25} (Fig. 3), yielding methionine sulfoxide, which is known to inhibit CNBr cleavage. The second peak showed a mass of 3352.8 Da, which was almost exactly the mass calculated for the expected pyridylethylated N-terminal fragment CB 1 (Fig. 3), 335 3Da. This was confirmed by amino acid sequence analysis. Peak 3 yielded a mass of 2251 Da and amino-acid sequence analysis confirmed that it contained the expected C-terminal fragment. Using modified sequencer cycles with cleavage temperature increased from 48°C to 53°C at Edman cycles corresponding to sequence positions P33 to C36 enabled us to identify amino acids C26 to I40 (Fig. 3 *A*). The calculated mass for the complete pyridylethylated sequence was 2114 Da, which was 137 Da less than the mass determined by ESI-MS. Because this is exactly the mass of a histidine, we assumed that the C-terminal amino acid was a histidine that had not been detected in amino-acid sequence analysis because of the combined overlap of His^{35} and His^{39} into the following cycles despite of the use of modified cycles to enhance cleavage at the P33-P34 bond. The complete sequence thus contained 41 amino acids and the calculated mass almost exactly matched the determined mass, assuming four disulfide bonds between the eight cysteines (calculated 4785.6 Da, measured 4785.2 Da).

The most frequent amino acid in this short sequence was cysteine with 19.5% of all amino acids, followed by histidine with 17% and arginine with 14.6%. The positively charged amino acids were almost counterbalanced by negatively charged ones and the calculated isoelectric point was 7.86. A comparison of the perlinhibin sequence to other protein sequences in data banks did not yield a convincing match. The short, cysteine-rich sequence aligned to other cysteine-rich sequences, preferably to metallothionin sequences of various organisms.

Isolation and partial sequence analysis of a perlinhibin-related polypeptide

During the purification of another nacre protein, we found, as one contamination of that protein among others, a polypeptide

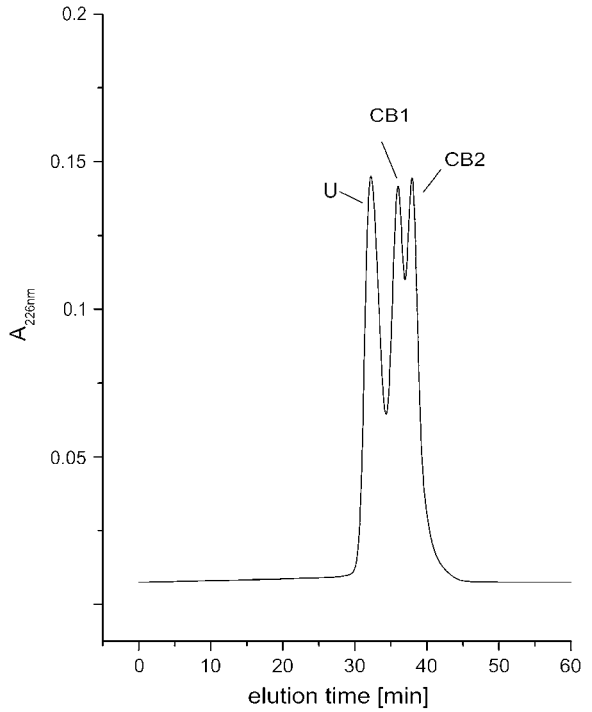

FIGURE 2 Size exclusion chromatographic separation of perlinhibin and its CNBr fragments. *CB1* and *CB2* are the N-terminal and C-terminal fragments, respectively, resulting from cleavage with CNBr. *U* is an uncleaved form of perlinhibin rendered resistant to CNBr cleavage from the oxidation of its single methionine.

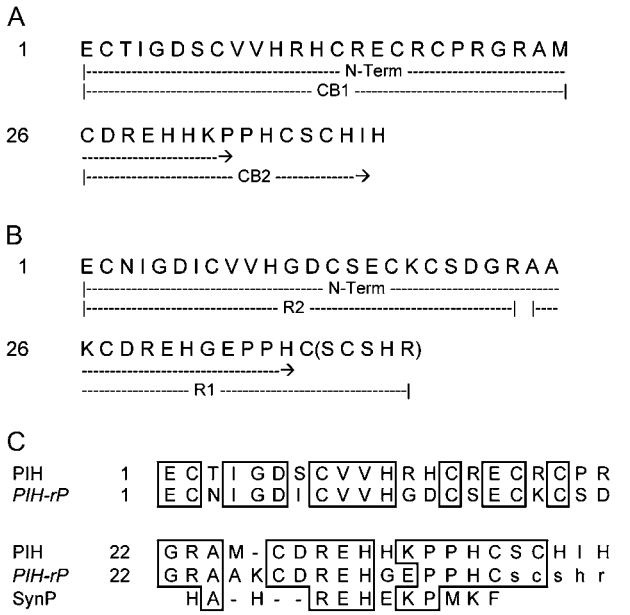

FIGURE 3 Amino-acid sequences of perlinhibin and perlinhibin-related protein. Broken lines indicate the sequenced peptides obtained after cleavage with CNBr (*CB*) or endoproteinase Arg-C (*R*). (*A*) The amino-acid sequence of perlinhibin. The C-terminal His was inferred from mass determination. (*B*) The amino-acid sequence of a perlinhibin-related protein. The last five amino acids (shown in *brackets*) are probable but not unequivocal identifications. (*C*) Alignment of the related sequences and the sequence of a chemically synthesized aragonite-binding peptide from Belcher and Gooch (6).

with an N-terminal amino-acid sequence very similar to that of perlinhibin. This perlinhibin-related protein was isolated after pyridylethylation of the mixture and rechromatography of the pyridylethylated proteins. The yield was ~0.04 μg/shell. Analysis of the entire sequence was complicated by the same problems as the analysis of perlinhibin. Enzymatic cleavage, reversed phase HPLC, and sequence analysis of the cleavage products yielded the amino-acid sequence shown in Fig. 3 *B*, but confirmation by mass spectrometry was not possible due to the lack of material. 67.5% of the sequence, including the eight cysteines, was identical to that of perlinhibin (Fig. 3, *B* and *C*). However, the number of basic residues (including His, which is only partially charged around neutral pH) was reduced and the number of acidic residues was increased.

Crystal growth inhibition by perlinhibin

The nanometer scale effect of perlinhibin on a specific calcite surface was examined in situ by atomic force microscopy. A freshly cleaved calcite surface ([4 $\overline{4}$ $\overline{1}$] plane) was incubated with a saturated calcium carbonate solution (pH 8.2) containing perlinhibin (0.02 mg/ml). The investigation was carried out in contact-mode at room temperature (Fig. 4, *A–H*). Visible growth of new mineral monomolecular layers (*white arrows*), mostly parallel to each other, started immediately and was followed by formation of holes, which progressively deepened and increased in diameter, as crystal growth continued. The formation of holes (*black arrows*) suggested that inhibition of mineral growth took place due to the adhesion of perlinhibin molecules to the calcite step-edges suppressing crystal growth. Step edges became therefore more frayed. Progressive overgrowth of calcite layers surrounding the binding sites led to a deepening of the holes and augmentation of their size. A progressive convolution of the mineral layers was also detectable (Fig. 4, *G–H*).

Further AFM investigations were carried out again, incubating a freshly cleaved calcite surface ([4 $\overline{4}$ $\overline{1}$] cleavage plane) with 0.02 mg/ml perlinhibin dissolved in a saturated calcium carbonate solution at pH 8.2 (Fig. 4, *I–L*).

The cleaved calcite sample was initially imaged at room temperature in deionized water. The surface presented several steps, which may be due to an imperfect cleavage or to crystal defects (Fig. 4 *I*). Dissolution of monomolecular layers took place as expected. While imaging, the aqueous solution in the fluid cell was exchanged against the calcium carbonate solution supplemented with perlinhibin. After 2 min incubation the surface appeared covered with white spots, corresponding to single perlinhibin molecules or protein aggregates. An initial growth of the mineral monomolecular layers over the preexisting one (Fig. 4 *J*, *white arrows*) and their convolution of the step edges were again

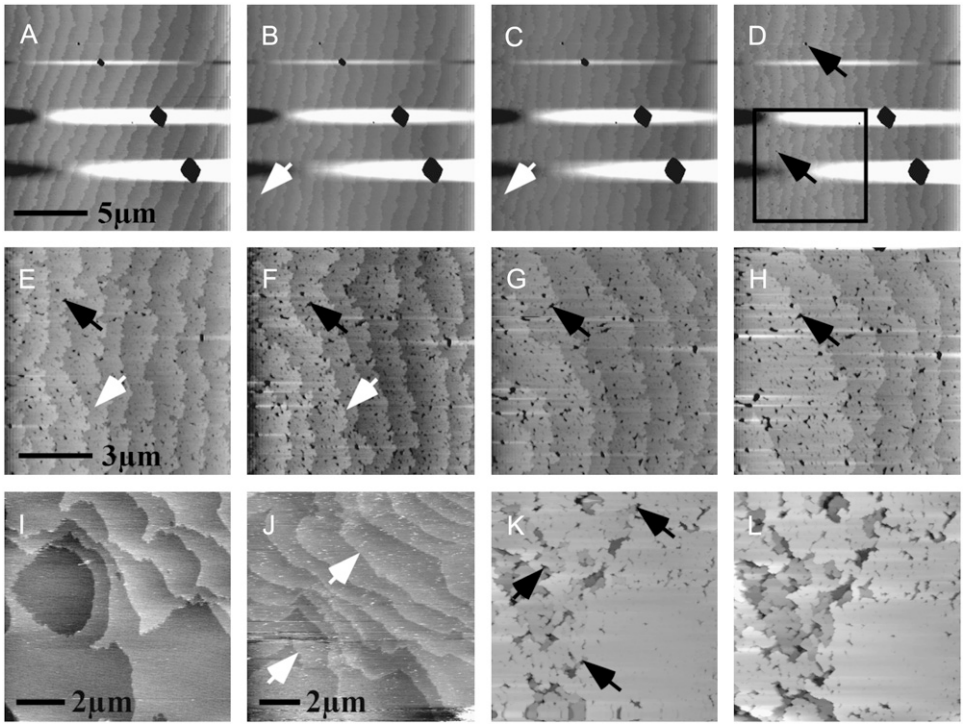

FIGURE 4 AFM investigation of the interaction of perlinhibin with geological calcite on a defined cleavage plane [4 $\bar{4}$ $\bar{1}$]. (*A–H*) Images of a geological calcite surface incubated with a saturated $CaCO_3$ solution containing 0.02 mg/ml perlinhibin (frames 1 min apart). Growth of mineral layers (*white arrows*) and formation of holes (*black arrows*) are shown. Due to perlinhibin adhesion to calcite steps, the growth at these spots is inhibited. (*E*) Higher magnification of the area delineated in panel *D* by a black rectangle. (*E–H*) Monomolecular calcite layers grow around the spots where perlinhibin is bound, leaving holes by overgrowing the underlying layers devoid of perlinhibin. (*I*) The calcite surface is imaged in deionized water. The fluid cell was initially filled with deionized water and the freshly cleaved calcite surface was imaged in contact-mode at room temperature. (*J–L*) Calcite surface incubated with a saturated $CaCO_3$ solution containing 0.02 mg/ml perlinhibin (pH 8.2) at room temperature. (*J*) The same surface as in panel *I* imaged after 2 min of incubation with saturated $CaCO_3$ solution containing perlinhibin. Formation of new monomolecular layers over the preexisting ones is visible (*white arrows*). (*K*) The same area imaged after 5 h. Formation of holes is visible. Hole formation (*black arrows*) is the direct consequence of perlinhibin adhesion to calcite steps and ensuing inhibition of crystal growth. Mineral binding only takes place at surfaces devoid of perlinhibin. (*L*) Surface after 10 h incubation with saturated $CaCO_3$ solution and perlinhibin. Height scale: black to white, 4 nm (*A–J*), 70 nm (*K* and *L*).

detectable (Fig. 4 *J*). The layers initially grew mostly parallel to each other as previously observed. After 5 h of incubation (Fig. 4 *K*) the growing monomolecular layers became confluent, inducing the formation of a mostly flat homogenous layer. The newly formed surface was again characterized by deep holes (*black arrows*). Enhancing of the mineral steps was visible and again suggested to be the direct consequence of perlinhibin adhesion to calcite steps and inhibition of calcium carbonate growth at the adhesion point. Growth of new layers was only possible where perlinhibin was not bound. The initial surface features were no longer recognizable, indicating that perlinhibin caused morphological alteration of the surface. The final state of the newly formed surface (after 10 h incubation, Fig. 4 *L*) was characterized by a further increase of the holes in size, diameter, and depth.

XRD investigation

The calcite crystal, after AFM investigation in a saturated $CaCO_3$ solution containing perlinhibin, was further investigated by x-ray diffraction. The diffraction pattern (Fig. 5) showed several peaks corresponding to calcite ($2\theta = 29.6°$), aragonite ($2\theta = 26.48°$), and mica ($2\theta = 8.5°$, 17.4°, 35.66°, and 45.14°). The peak corresponding to aragonite clearly indicated that perlinhibin induced the polymorph transition at ambient conditions in vitro. Although, compared to the whole crystal sample, crystal overgrowth was thin, the aragonite peak was almost as high as the calcite peak. This was presumably caused by the limited penetration depth of the x rays, resulting in a diffraction pattern where crystal parts close to the surface are emphasized. Interestingly, only a single aragonite peak was present, whereas an aragonite powder spectrum is composed of several peaks of similar height. It is possible that the newly nucleated layers were at least semioriented since they were grown on a single crystalline substrate. Thus they deviate from an aragonite powder pattern. The mica peaks were induced by the sample holder, which was used for AFM investigation.

Inhibition of crystal dissolution in calcium chloride solution by perlinhibin

To examine the specific interaction of perlinhibin with a calcite surface in more detail, a freshly cleaved calcite surface was incubated with perlinhibin dissolved in calcium chloride solution, which does not support crystal growth. Freeze-dried perlinhibin was dissolved in a 7.5 mM $CaCl_2$ solution (pH 7.5) to a final concentration of 0.02 mg/ml.

The freshly cleaved calcite surface was initially imaged in deionized water for several minutes (Fig. 6 *A*). The calcite surface presented the characteristic rhombohedral voids with a depth of ~0.40 nm, which correspond to singular

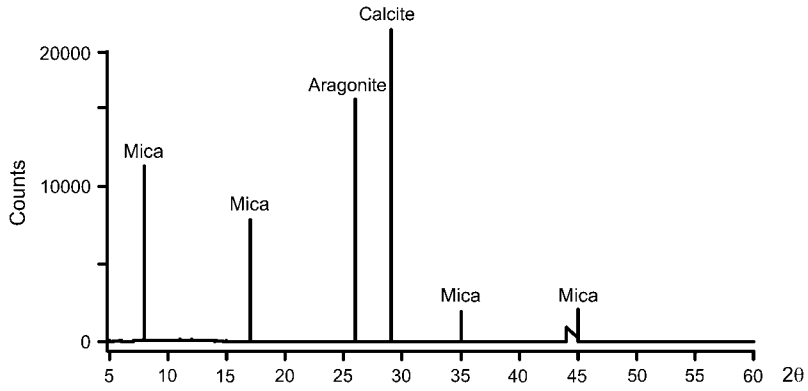

FIGURE 5 XRD diffraction pattern of geological calcite incubated for 20 h with a saturated $CaCO_3$ solution (pH 8.2) containing perlinhibin (0.02 mg/ml). The presence of the aragonite peak indicates that perlinhibin induced formation of aragonite on the calcite substrate. The formation of aragonite can only be due to perlinhibin, because formation of aragonite at room temperature and in the absence of magnesium ions or other additives is never observed. The peaks corresponding to mica, a silicate, were caused by the sample holder.

monomolecular calcite layers. The spontaneous dissolution of calcium carbonate layers took place as previously observed (17). After 20 min, the aqueous solution in the fluid cell was exchanged against the calcium chloride solution supplied with perlinhibin. Flushing-in induced perturbations in the fluid cell and a progressive sample drift along the upper-right direction (Fig. 6, *B* and *C*). A visible modification of the calcite surface took place at the edges (Fig. 6, *white arrows*), while the surfaces of the layers remained unmodified. Single perlinhibin molecules, which appeared as small white spots, bound progressively to the crystal edges, inhibiting, at that point, the dissolution of the layers.

During this investigation, the contours of the layers became highlighted and more enhanced in the vertical direction, due to a progressive binding of the proteins at calcium carbonate edges. Convolution of the calcite monomolecular layer was observed again. After 25 min of incubation, visible variations of the surface morphology were no longer detected (Fig. 6, *F–I*), suggesting that perlinhibin suppressed any kind of process taking place on the calcite surface.

By measuring the height of the ridges, we estimated the calcite step ridge enhancement caused by adhesion of perlinhibin molecules (Fig. 7). Where no proteins were bound, a step height of 0.35 nm was observed, which corresponds to the typical size of a monomolecular calcite layer. A step enhancement of ~0.5 nm was observed at the perlinhibin binding sites.

De novo crystal growth by vapor diffusion technique

The role of perlinhibin in nucleation and growth of calcium carbonate crystals was investigated with the ammonium carbonate vapor diffusion technique. Scanning electron microscope investigation showed that, in the absence of protein, only calcite rhombohedra of ~20 μm in size were formed (Fig. 8 *A*). When crystallization was carried out in the presence of perlinhibin (0.02 mg/ml), crystals and crystal aggregates of different sizes (from ~10 to 100 μm) formed

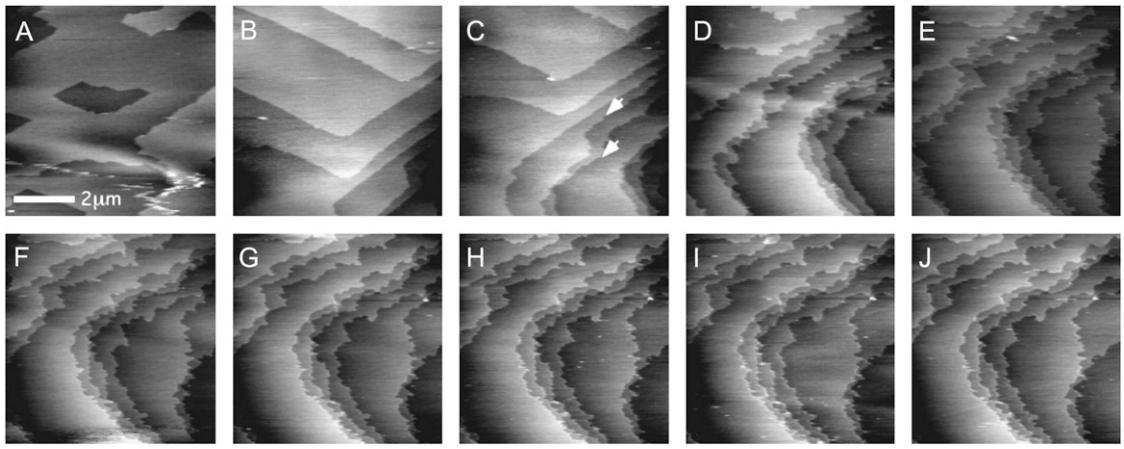

FIGURE 6 Consecutive AFM images of geological calcite surface cleaved along the [4 $\bar{4}$ $\bar{1}$] plane. (*A*) Calcite surface imaged in deionized water, dissolution of the crystal is visible. (*B–J*) Frames 3-min apart, consecutive images of the same calcite surface incubated with a 7.5 mM $CaCl_2$ solution containing perlinhibin (0.02 mg/ml). Perlinhibin binds specifically to calcite steps preventing the dissolution of the calcite layers where it is bound. In 7.5 mM $CaCl_2$ solution, the surface of a calcite crystal dissolves slowly. As single perlinhibin molecules bind to the steps (*white spots*), they protect the binding region against further dissolution; however, this dissolution continues at sites without bound protein, leading to frayed ridges. Height scale: black to white, 4 nm.

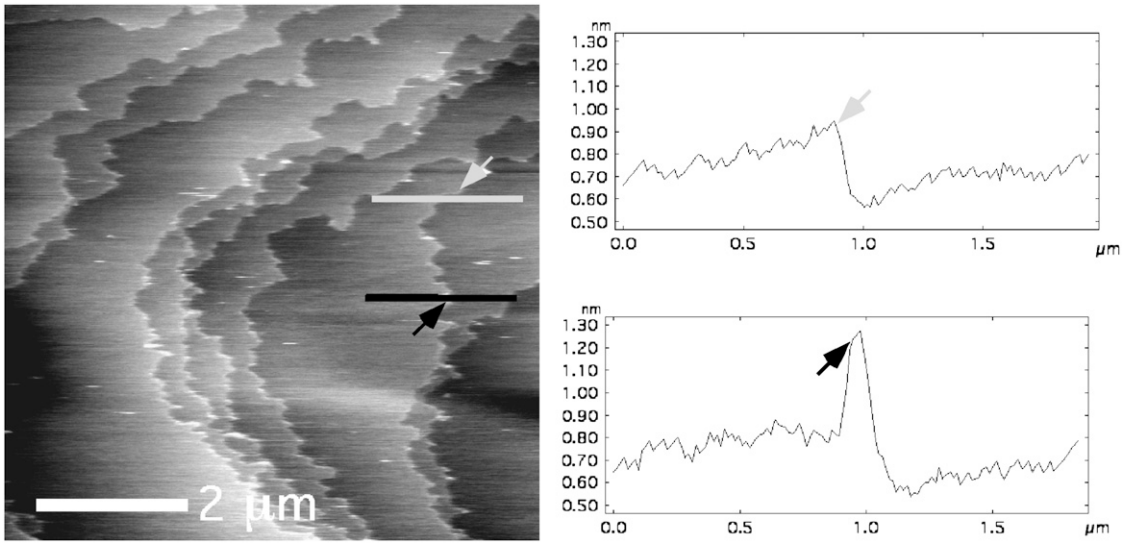

FIGURE 7 Atomic force microscopic image of a calcite surface incubated with perlinhibin. Perlinhibin is bound at some spots of the step ridges of monomolecular layers. Perlinhibin appears as very small spots of a height of ~0.6–0.8 nm (see *lower line plot* on the *right side*). The open line marks an edge without bound perlinhibin, the black line marks an edge with bound perlinhibin. The black line is drawn directly over a bound protein molecule. The corresponding line plots are shown at the right side. The upper line plot shows the height of a monomolecular step at the calcite crystal surface. The step height is ~0.35 nm, which corresponds nicely to the actual value of 0.32 nm and shows that the instrument is well calibrated. The lower line plot drawn over a bound perlinhibin molecule shows a height of ~0.5 nm for the perlinhibin binding site.

(Fig. 8, *B–E*). Crystals were characterized by a rhombohedral-cubic habit. This morphology, similar to that of calcite crystals, suggested that mainly the most thermodynamically stable polymorph nucleated. The crystal faces appeared highly corrugated; the nucleation of new layers with an irregular, convoluted shape took place on the preexisting layers. The crystals showed the presence of deep pits, suggesting that perlinhibin inhibited the crystal growth at the binding sites and that crystallization was only possible around the surface covered by perlinhibin. Due to the lack of material, it was not possible to study the influence of perlinhibin-related protein on calcium carbonate crystallization.

DISCUSSION

To understand the growth of nacre, which takes place in an extracellular space delimited by a preformed organic matrix, it seems promising to identify and purify the major organic components of the organic matrix and to study their effect on calcium carbonate crystallization. In the course of our ongoing search for new matrix components, we isolated a small matrix protein with previously unknown amino-acid sequence. Because of its inhibitory effect on calcium carbonate crystallization the protein was named perlinhibin. In contrast to other biomineralizing proteins from abalone nacre sequenced

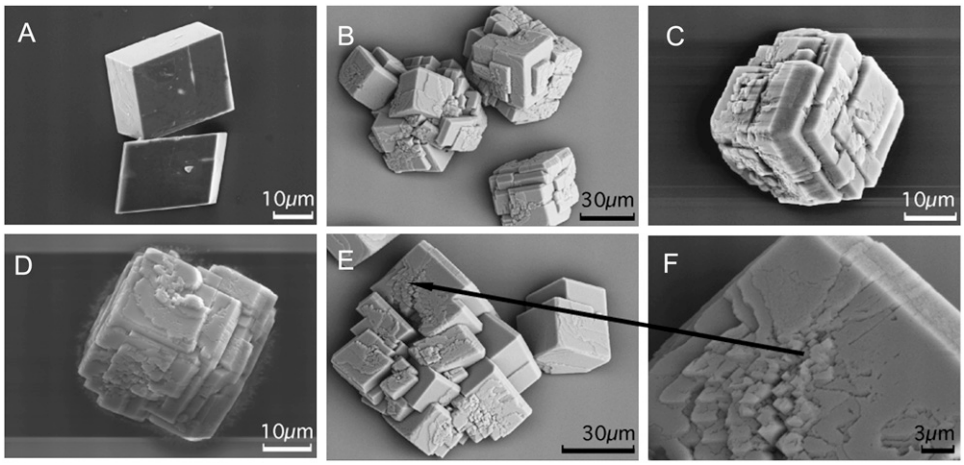

FIGURE 8 SEM images of calcium carbonate crystals precipitated using the ammonium carbonate method in the absence (*A*) or presence (*B–F*) of perlinhibin. (*A*) Dishes containing 7.5 mM $CaCl_2$ solution (pH 7.5) in an airtight desiccator were exposed to ammonium carbonate vapor for five days at room temperature. The precipitated crystals grew with the typical morphology of geological calcite. (*B–F*) Dishes with 7.5 mM $CaCl_2$ solution (pH 7.5) containing perlinhibin (0.02 mg/ml of protein) in an airtight desiccator were exposed to ammonium carbonate vapor for five days at room temperature. Perlinhibin caused inhibition of crystal growth at the binding site. The precipitated crystals showed many steps and holes. (*F*) Hole formation caused by adhesion of perlinhibin can be observed at higher magnification.

before, the sequence of this new protein did not belong to a previously known family and did not include a known motif such as the C-type lectinlike domain of perlucin (11), the IGF-binding domain of perlustrin (12), or the whey acidic protein domains of perlwapin (13). However, abalone nacre also contained a perlinhibin-related protein showing a sequence identity of 67.5% to perlinhibin, indicating that these new small proteins may belong to a family of closely related nacre matrix proteins. While a database search with the new sequences was not very productive, the comparison to a group of small synthetic peptides binding to aragonite (6), the calcium carbonate polymorph occurring in nacre, was potentially interesting (Fig. 3 *C*). The stretch of protein sequence similar to this aragonite-binding peptide may be part of a mineral-binding motif of perlinhibin. Our results showed that nacre matrix proteins interacting with the mineral phase need not necessarily be highly acidic. Probably the proper spacing of positively charged and negatively charged residues and of histidine, which has a pK_a of the side chain near 6 and is protonated only to a low extent at neutral pH, is more important than overall acidity.

AFM experiments on a calcite surface showed that perlinhibin specifically bound to calcite steps whereas, on the monomolecular faces, only unbound perlinhibin (visible as small dots) was observable, with positions changing in consecutive images taken of the same spot. Because of this step adsorption of the protein, the dissolution and growth mechanism of the calcite surface, which takes place by movement of steps, was highly altered. Dissolution of the crystal was inhibited at the binding sites, leaving a frayed surface (Figs. 5 and 6) and the growth of calcite was consistently inhibited at the protein-binding sites (Fig. 4) causing the formation of holes. These observations were supported by crystallization experiments performed with the ammonium carbonate vapor diffusion technique in presence of perlinhibin. Crystals were obtained which, morphologically, roughly resembled calcite. The surface of these crystals was covered with pits presumably due to perlinhibin binding. New layers were nucleated possibly because of the disturbance that was caused by the perlinhibin binding.

XRD investigation of a calcite crystal after AFM investigations with a supersaturated calcium-carbonate solution in presence of perlinhibin showed that the crystal overgrowth consisted of aragonite. Before, only the mixture of water-soluble nacre proteins was known to cause such a transition (18), but until now no isolated abalone nacre protein was identified to cause this polymorph change. A possible but speculative explanation for these findings might be that perlinhibin specifically inhibits calcite growth by making the growth energetically unfavorable, and thus indirectly promotes the growth of aragonite (the third water free calcium carbonate polymorph, vaterite, usually only develops upon rapid crystallization).

The possible role of inhibitory proteins like perlinhibin or perlwapin in abalone nacre formation might be the prevention of uncontrolled mineralization of calcite inside the extrapallial fluid. Other organic matrix components like perlucin and the water-insoluble organic matrix, which forms a three-dimensional framework before mineralization, are responsible for nucleation and spatial alignment of crystallization (19). However, it is likely that in nature, the situation is more complex, and at least some of the organic components have multiple roles; for example, modulation of crystallization and connection of mineral and organic components.

The protein sequence data reported in this work will appear in the Uniprot Knowledgebase under the accession numbers P85035 (perlinhibin) and P85036 (perlinhibin-related protein).

We are grateful to Fabienne Bosselmann, University of Duisburg-Essen, Germany, who performed the x-ray diffraction measurements.

REFERENCES

1. Lowenstam, H. A., and S. Weiner. 1989. On Biomineralization. Oxford University Press, New York.
2. Simkiss, K., and K. M. Wilbur. 1989. Biomineralization. Cell Biology and Mineral Deposition. Academic Press, San Diego.
3. Wheeler, A. P., J. W. George, and C. A. Evans. 1981. Control of calcium carbonate nucleation and crystal growth by soluble matrix of oyster shell. *Science*. 212:1397–1398.
4. Addadi, L., and S. Weiner. 1985. Interactions between acidic proteins and crystals: stereochemical requirements in biomineralization. *Proc. Natl. Acad. Sci. USA*. 82:4110–4114.
5. Fritz, M., and D. E. Morse. 1998. The formation of highly organized biogenic polymer/ceramic composite materials: the high-performance microlaminate of molluscan nacre. *Curr. Opinion Coll. Surf. Sci.* 3:55–62.
6. Belcher, A. M., and E. E. Gooch. 2000. From biology to biotechnology and medical application. *In* Biomineralization. E. Baeuerlein, editor. Wiley-VCH, Weinheim.
7. Belcher, A. M., X. H. Wu, R. J. Christensen, P. K. Hansma, G. D. Stucky, and D. E. Morse. 1996. Control of crystal phase switching and orientation by soluble mollusk-shell proteins. *Nature*. 381:56–58.
8. Walters, D. A., B. L. Smith, A. M. Belcher, G. T. Paloczi, G. D. Stucky, D. E. Morse, and P. K. Hansma. 1997. Modification of calcite crystal growth by abalone shell proteins: an atomic force microscope study. *Biophys. J.* 72:1425–1433.
9. Shen, X., A. M. Belcher, P. K. Hansma, G. D. Stucky, and D. E. Morse. 1997. Molecular cloning and characterization of lustrin A, a matrix protein from shell and pearl nacre of *Haliotis rufescens*. *J. Biol. Chem.* 272:32472–32481.
10. Smith, B. L., T. E. Schäffer, M. Viani, J. B. Thompson, N. A. Frederick, J. Kindt, A. M. Belcher, G. D. Stucky, D. E. Morse, and P. K. Hansma. 1999. Molecular mechanistic origin of the toughness of natural adhesives, fibers and composites. *Nature*. 399:761–763.
11. Mann, K., I. M. Weiss, S. André, H.-J. Gabius, and M. Fritz. 2000. The amino-acid sequence of the abalone (*Haliotis laevigata*) nacre protein perlucin. Detection of a functional C-type lectin domain with galactose/mannose specificity. *Eur. J. Biochem.* 267:5257–5264.
12. Weiss, I. M., W. Göhring, M. Fritz, and K. Mann. 2001. Perlustrin, a *Haliotis laevigata* (abalone) nacre protein is homologous to the insulin-like growth factor binding protein N-terminal module of vertebrates. *Biochem. Biophys. Res. Commun.* 285:244–249.
13. Treccani, L., K. Mann, F. Heinemann, and M. Fritz. 2006. Perlwapin, an abalone nacre protein with three four-disulfide core (whey acidic protein) domains, inhibits the growth of calcium carbonate crystals. *Biophys. J.* 91:2601–2608.
14. Michenfelder, M., G. Fu, C. Lawrence, J. Weaver, B. Wustman, L. Taranto, J. S. Evans, and D. Morse. 2003. Characterization of two

molluscan crystal-modulating biomineralization proteins and identification of putative mineral binding domains. *Biopolymers*. 70:522–533.

15. Fu, G., S. Valiyaveettil, B. Wopenka, and D. Morse. 2005. $CaCO_3$ biomineralization: acidic 8-kDa proteins isolated from aragonitic abalone shell nacre can specifically modify calcite crystal morphology. *Biomacromolecules*. 6:1289–1298.
16. Weiss, I. M., S. Kaufmann, K. Mann, and M. Fritz. 2000. Purification and characterization of perlucin and perlustrin, two new proteins from the shell of the mollusk *Haliotis laevigata*. *Biochem. Biophys. Res. Commun*. 267:17–21.
17. Hillner, P. E., A. J. Grats, S. Manne, and P. K. Hansma. 1992. Atomic scale imaging of calcite growth and dissolution in real time. *Geology*. 20:359–362.
18. Thompson, J., G. Paloczi, J. Kindt, M. Michenfelder, B. Smith, G. D. Stucky, D. Morse, and P. K. Hansma. 2000. Direct observation of the transition from calcite to aragonite as induced by abalone shell proteins. *Biophys. J*. 79:3307–3312.
19. Heinemann, F., L. Treccani, and M. Fritz. 2006. Abalone nacre insoluble matrix induces growth of flat and oriented aragonite crystals. *Biochem. Biophys. Res. Commun*. 344:45–49.